

THE MULTI-FUNCTIONAL MODELLING SHEAR LAG METHOD FOR ACCURATE CALCULATION OF STATIC RESPONSE AND ACCORDION EFFECT OF IMPROVED COMPOSITE BOX GIRDERS

YA-NAN GAN¹, ZI-CHEN ZHANG^{2*}, GEN-HUI WANG²

¹*School of Civil Engineering and Architecture, Yancheng Institute of Technology, Yancheng, China*

²*School of Civil Engineering and Architecture, Lanzhou Jiaotong University, Lanzhou, China*

Received 17 September 2021; accepted 18 August 2022

Abstract. The composite box girder with corrugated web and steel bottom plate (CW-SBS) is a kind of improved steel-concrete structures. The design of CW-SBS box girders needs the accurate method to calculate the working response and accordion effect in consideration of the self-stress equilibrium condition of shear lag warping stress and shear deformation. This study proposes the multi-functional modelling shear lag (MFMSL) method which adopts the four longitudinal displacement difference functions to model the variation of shear lag in the CW-SBS box girders with different wing slab widths and thicknesses. Therefore, MFMSL is a method to calculate the static response and accordion effect of the CW-SBS composite box girders. Structural differential equations based on the energy-variation principle present that the MFMSL method effectively improves the calculating accuracy of the CW-SBS box girder static

* Corresponding author. E-mail: yxm4655@163.com

Ya-Nan GAN (ORCID ID 0000-0002-0158-8542)
Zi-Chen ZHANG (ORCID ID 0000-0003-2183-9203)
Gen-Hui WANG (ORCID ID 0000-0002-5129-6070)

Copyright © 2023 The Author(s). Published by RTU Press

This is an Open Access article distributed under the terms of the Creative Commons Attribution License (<http://creativecommons.org/licenses/by/4.0/>), which permits unrestricted use, distribution, and reproduction in any medium, provided the original author and source are credited.

response, which can be verified by both experimental and simulative results. Also, the MFMSL method demonstrates that the accordion effect of the CW-SBS box girder is stronger than that of the traditional composite box girder and closely relates to the load distribution. Hence, the proposed method further lays the foundation for the analysis and design of CW-SBS box girders.

Keywords: accordion effect, energy-variation principle, improved composite box girder, MFMSL method, self-stress equilibrium condition, shear lag.

Introduction

So far, the prestressed concrete (PC) box girder has been widely used in bridge engineering (Gomez et al., 2011; Zeying et al., 2015; Zhang et al., 2017), but its mechanical and material defects have gradually appeared, many PC box girders have stiffness degradation and beam cracking (He et al., 2021; Limongelli et al., 2018; Zhao et al., 2022). In order to weaken the restraint behaviour of flange and web of PC box girder, French scholars proposed using corrugated steel web instead of PC box girder web, and took the lead in building a cognac bridge in 1986. Since then, a large number of composite box girder bridges with corrugated steel webs have been built (Mo et al., 2000; Yong et al., 2012). For example, Germany built the Altwipfergund Bridge in 2001, Hungary built the Móra Ferenc Bridge in 2011, Japan built the Yasukawa Bridge in 2004, and Venezuela built the Caracas Bridge. Besides, the developing transportation in the world promotes the larger width and span of bridge deck to achieve greater engineering benefits. Therefore, the box girder bridge with a multi-box chamber presents a wider application prospect (Kim et al., 2013; Shen et al., 2018). Since the construction of the Cognac Bridge in 1986, the multi-chamber composite box girder bridges have been widely built in highway engineering around the world, such as the Kurobegawa Bridge completed in 2006.

Particularly, this kind of bridges has been built more in the infrastructures of China in recent years (Chen et al., 2019; Zhou et al., 2019), such as Shenzhen Nanshan Bridge in 2011 and Shanxi Yunbao Yellow River Bridge in 2019. In the engineering practice, the bridge experts gradually realised that the bottom flange (RC slab) of the traditional corrugated steel web composite box girder should be replaced by the flat steel plate and could be taken as an improved type of steel-concrete structures with the advantages such as lighter self-weight, higher prestressing efficiency, stable mechanical performance and large span capacity. Particularly, because of the accordion effect of corrugated steel web, the improved composite box girder with a double box and a single chamber can effectively avoid the bridge diseases caused by shrinkage, creep and temperature effect (Zhou et

al., 2016; Elgaaly et al, 1997; Oh et al., 2012). The structural weight is further reduced by about 50%, when compared with the traditional PC box girders. The advantage of improved composite box girder is more conducive to the increasing of the width and span of the composite girder bridge. The western and coastal areas of China have adopted this kind of improved simply supported and continuous composite box girder bridges, for instance, two bridges shown in Fig. 1.

Accordingly, the research on this kind of composite structures also becomes an important aspect in the field of bridge engineering (He et al., 2012; Aparna et al., 2020). In fact, although the improved type of composite box girders is under construction, the studies on analytical theories and key technologies still need to be developed to deal with the problems derived by the specific working characteristics of composite structures (Deng et al., 2021; Jiang et al., 2014). For example, compared with the traditional composite box girder, the mass of the improved composite box girder is more in the roof and results in stronger transverse asymmetry, so that it is necessary to introduce the self-stress equilibrium condition of the shear lag warping stress. Therefore, this study establishes the elastic control differential equation of improved composite box girder considering the accordion effect, Timoshenko shear deformation and shear lag warping stress self-equilibrium. Then the static characteristics of improved composite box girders are revealed through the solution of the control differential equation, which could provide the reference to the design improvement.



Figure 1. CW-SBS composite box girder at Gansu Province in China: (a) Terminal 2 connecting line continuous beam bridge at Zhongchuan Airport, (b) the construction of Dunhuang to Dangjin mountain Expressway bridge

1. Control differential equation and boundary condition of CW-SBS box girder

The research is carried out through theoretical derivation, numerical simulation and experimental exploration. Accordion effect, shear lag and self-equilibrium condition of shear lag warping stress are considered in the theoretical analysis. The theoretical basis of this paper is more solid.

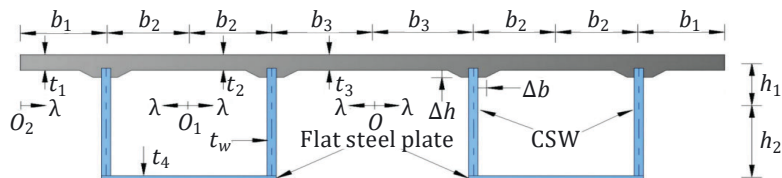
1.1. Equivalent geometric dimension of steel bottom plate

When the CW-SBS box girder is in vertically bending state, its steel bottom plate can be converted into the imaginary section area of tension concrete, i.e., $A_4 = \alpha_{Es}A_t$ and $\alpha_{Es} = E_s/E_c$, where E_c is the elastic modulus of concrete slab; E_s is the elastic modulus of steel bottom plate; A_t is the cross-sectional area of steel bottom plate. Moreover, due to the difference between Poisson's ratios of steel and concrete, the shear strain energy calculation of the steel bottom plate can be converted into: $A_{sG} = \alpha_{Gs}A_s$, $\alpha_{Gs} = G_t/G_c$, where G_c and G_t are the shear modulus values of concrete slab and steel bottom plate, respectively.

1.2. The longitudinal warping displacement function for flanges

In order to analyse the mechanical properties of the improved composite box girder, the local coordinate system with origin O , O_1 and O_2 is established (Figure 2a). Figure 2 shows that a CW-SBS box girder

a) Cross section and local coordinate system



b) Coordinate and load system

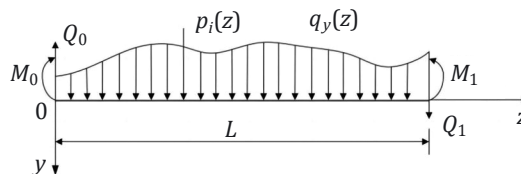


Figure 2. A CW-SBS box girder with corrugated steel webs

with corrugated steel webs yields the flexure response in the y - z plane under the distributed load (Figure 2b). $w(z)$ and $\Theta(z)$ are the vertical deflection of the box girder and the vertical corner of the section; $u_1(z)$, $u_2(z)$, $u_3(z)$ and $u_4(z)$ are the longitudinal displacement difference functions of cantilever slab (b_1), upper flange (b_2 , b_3) and lower flange, respectively. Correspondingly, the longitudinal displacements U_1 , U_2 , U_3 , and U_4 are the sum of the box girder flange warping displacements, $M_{01}u_1$, $M_{02}u_3$, $M_{03}u_3$ and $M_{04}u_4$, caused by the shear lag effect and the displacements of rigid section. M_{01} , M_{02} , M_{03} and M_{04} are the constant coefficients obtained by the shear lag warping stress self-equilibrium condition. Thus, the longitudinal displacement at any point on the cross section of the box girder can be obtained. Based on this aspect, the stress of the improved composite box girder can be given.

1.3. Total energy in a CW-SBS box girder

Based on the mechanical characteristics of CW-SBS box girder, it is possible to calculate the total stress values of cantilever slab (part b_1), upper flange (part b_2) and bottom steel plate (part b_2) in consideration of shear lag and accordion effect. Then, according to the stress expressions, the total strain energy in the top and bottom flanges can be calculated:

$$\begin{aligned}
 V_1 = & \frac{E}{2} \int_0^l I(\theta')^2 dz + \frac{E}{2} \int_0^l I_1(u_1')^2 dz + \frac{E}{2} \int_0^l I_2(u_2')^2 dz + \frac{E}{2} \int_0^l I_3(u_3')^2 dz + \\
 & \frac{E}{2} \int_0^l I_4(u_4')^2 dz + \frac{E}{2} \int_0^l I_5(\theta'u_1')^2 dz + \frac{E}{2} \int_0^l I_6(\theta'u_2')^2 dz + \frac{E}{2} \int_0^l I_7(\theta'u_3')^2 dz + \\
 & \frac{E}{2} \int_0^l I_8(\theta'u_4')^2 dz + \int_0^l EI_9 u_1' u_2' dz + E \int_0^l I_{10} u_1' u_3' dz + E \int_0^l I_{11} (u_1' u_4') dz + \\
 & E \int_0^l I_{12} (u_2' u_3') dz + E \int_0^l I_{13} (u_2' u_4') dz + E \int_0^l I_{14} (u_3' u_4') dz + \frac{G}{2} \int_0^l I_{G1} (u_1')^2 dz + \\
 & \frac{G}{2} \int_0^l I_{G2} (u_2')^2 dz + \frac{G}{2} \int_0^l I_{G3} (u_3')^2 dz + \frac{G}{2} \int_0^l I_{G4} (u_4')^2 dz
 \end{aligned} \tag{1}$$

where $I = \int_{A_1} y^2 dA_1 + \int_{A_2} y^2 dA_2 + \int_{A_3} y^2 dA_3 + \int_{A_4} y^2 dA_4$; $I_{G1} = \frac{\pi^2 h_1^2 t_1}{4b_1}$; $I_{G2} = \frac{\pi^2 h_1^2 t_2}{2b_2}$;

$$I_{G3} = \frac{\pi^2 h_1^2 t_3}{4b_3}; I_{G4} = \frac{\pi^2 h_2^2 \alpha_{Gs} t_4}{2b_2}.$$

According to the shear lag warping stress self-equilibrium condition, M_{01} , M_{02} , M_{03} and M_{04} can be obtained.

$$M_{01} = \frac{4h_1 b_1 t_1}{\pi A}, M_{02} = \frac{8h_1 b_2 t_2}{\pi A}, M_{03} = \frac{4h_1 b_3 t_3}{\pi A}, M_{04} = \frac{-8h_2 b_2 \alpha_{Es} t_4}{\pi A}$$

Here, $I_1 \sim I_{14}$ are the coefficients related to $M_{01} \sim M_{04}$, $I, b_1 \sim b_3, t_1 \sim t_4$ and π .

The shear strain energy of the CW-SBS box girder is

$$T_{zj} = \frac{1}{2} \int_0^l G_s A_s (w' - \theta)^2 dz \quad (2)$$

where A_s is the cross-sectional area of corrugated steel webs; G_s is the modified shear modulus of corrugated steel webs.

The external loading-induced potential energy V_p can be given by

$$V_p = - \int_0^l q_y(z) w(z) dz - [Q(z)w(z)] \Big|_0^l + [M_1(z)u_1(z) + M_2(z)u_2(z)] \Big|_0^l + \\ M_3(z)u_3(z) + M_4(z)u_4(z) + M_z(z)\theta(z) \Big|_0^l \quad (3)$$

Now, the total potential energy of the CW-SBS box girder can be calculated as follows:

$$V = V_1 + T_{zj} + V_p \quad (4)$$

where $M_1(z)$, $M_2(z)$, $M_3(z)$ and $M_4(z)$ are the bending moments about x -axis caused by the shear lag effect of flanges; $M_z(z)$ is the axial bending moment about axis x when the end of the girder has a vertical angle of $\theta(z)$; $Q(z)$ and $q_y(z)$ are the vertical shear force at the end of the girder and the vertical distributed force on the box girder; E and G are Young's and shear modulus of concrete, respectively; A_1 , A_2 and A_3 are the areas of the cantilever slabs (part b_1), top slab (part b_2), and top slab (part b_3) of the box girder, respectively; A_4 is the converted area of steel bottom plate, and $A = A_1 + A_2 + A_3 + A_4$; I is the moment of inertia of the cross section about the centroidal x -axis.

1.4. Governing differential equation and its solution

Up to now, according to the principle of minimum potential energy ($\delta V = 0$), the governing differential equations and natural boundary conditions of the CW-SBS box girder can be given as follows.

$$EI_5 \theta'' + EI_1 u_1'' + EI_9 u_2'' + EI_{10} u_3'' + EI_{11} u_4'' - GI_{G1} u_1 = 0 \quad (5)$$

$$EI_6 \theta'' + EI_9 u_1'' + EI_2 u_2'' + EI_{12} u_3'' + EI_{13} u_4'' - GI_{G2} u_2 = 0 \quad (6)$$

$$EI_7 \theta'' + EI_{10} u_1'' + EI_{12} u_2'' + EI_3 u_3'' + EI_{14} u_4'' - GI_{G3} u_3 = 0 \quad (7)$$

$$EI_8\theta'' + EI_{11}u_1'' + EI_{13}u_2'' + EI_{14}u_3'' + EI_4u_4'' - GI_{G4}u_4 = 0 \quad (8)$$

$$EI\theta'' + EI_5u_1'' + EI_6u_2'' + EI_7u_3'' + EI_8u_4'' + G_sA_s(w' - \theta) = 0 \quad (9)$$

$$G_sA_s(w'' - \theta') + q_y = 0 \quad (10)$$

$$\left[EI_5\theta' + EI_1u_1' + EI_9u_2' + EI_{10}u_3' + EI_{11}u_4' - M_1 \right]_0^l \delta u_1 = 0 \quad (11)$$

$$\left[EI_6\theta' + EI_9u_1' + EI_2u_2' + EI_{12}u_3' + EI_{13}u_4' - M_2 \right]_0^l \delta u_2 = 0 \quad (12)$$

$$\left[EI_7\theta'' + EI_{10}u_1'' + EI_{12}u_2'' + EI_3u_3'' + EI_{14}u_4'' - M_3 \right]_0^l \delta u_3 = 0 \quad (13)$$

$$\left[EI_8\theta' + EI_{11}u_1' + EI_{13}u_2' + EI_{14}u_3' + EI_4u_4' - M_4 \right]_0^l \delta u_4 = 0 \quad (14)$$

$$\left[G_sA_s(w' - \theta) - Q(z) \right]_0^l \delta w = 0 \quad (15)$$

By means of permutation between the differential Equations (5)–(10), the equation can be deduced as

$$u_1^{(9)} + \frac{R_3S_1 - R_1S_3 + (R_4 - S_4)}{R_3 - S_3} u_1^{(7)} + \frac{R_3S_2 - R_2S_3 + R_4S_1 - R_1S_4 + R_5 - S_5}{R_3 - S_3} u_1^{(5)} + \frac{R_4S_2 - R_2S_4 + R_5S_1 - R_1S_5}{R_3 - S_3} u_1^{(3)} + \frac{R_5S_2 - R_2S_5}{R_3 - S_3} u_1' + \frac{R_2S_6 - R_6S_2}{R_3 - S_3} q_y = 0 \quad (16)$$

where $R_1 \sim R_6$; $S_1 \sim S_6$ are the coefficients related to I , $I_1 \sim I_{14}$, $I_{G1} \sim I_{G4}$, E and G . Let us find the eigenvalues of Equation (16): $r_{1,2} = \pm\eta_1$, $r_{3,4} = \pm\eta_2$, $r_{5,6} = \pm\eta_3$ and $r_{7,8} = \pm\eta_4$. Then let us obtain the solution of Equation (17).

$$u_1(z) = c_1ch\eta_1z + c_2sh\eta_1z + c_3ch\eta_2z + c_4sh\eta_2z + c_5ch\eta_3z + c_6sh\eta_3z + c_7ch\eta_3z + c_8sh\eta_3z + c_9 \frac{-G_sA_sI_5}{GI_{G1}I} + c_{10} \frac{G_sA_sI_5}{GI_{G1}I} + \frac{-I_5}{GI_{G1}I} q_y z \quad (17)$$

Further, it is possible to derive the expressions of $u_2(z)$, $u_3(z)$ and $u_4(z)$ similar to Equation (17). By substituting Equation (17), $u_2(z)$, $u_3(z)$ and $u_4(z)$ into Equations (5)–(8), the constant coefficients of $u_2(z)$, $u_3(z)$ and $u_4(z)$ can be deduced according to the identity theorem. Thus, the solution of $u_2(z)$, $u_3(z)$ and $u_4(z)$ can be given by Equations (18)–(20).

$$u_2(z) = c_1B_1ch\eta_1z + c_2B_1sh\eta_1z + c_3B_3ch\eta_2z + c_4B_3sh\eta_2z + c_5B_5ch\eta_3z + c_6B_5sh\eta_3z + c_7B_7ch\eta_3z + c_8B_7sh\eta_3z + c_9 \frac{-G_sA_sI_6}{GI_{G2}I} + c_{10} \frac{G_sA_sI_6}{GI_{G2}I} + \frac{-I_6}{GI_{G2}I} q_y z \quad (18)$$

$$u_3(z) = c_1D_1ch\eta_1z + c_2D_1sh\eta_1z + c_3D_3ch\eta_2z + c_4D_3sh\eta_2z + c_5D_5ch\eta_3z + c_6D_5sh\eta_3z + c_7D_7ch\eta_3z + c_8D_7sh\eta_3z + c_9 \frac{-G_sA_sI_7}{GI_{G3}I} + c_{10} \frac{G_sA_sI_7}{GI_{G3}I} + \frac{-I_7}{GI_{G3}I} q_y z \quad (19)$$

$$u_4(z) = c_1E_1ch\eta_1z + c_2E_1sh\eta_1z + c_3E_3ch\eta_2z + c_4E_3sh\eta_2z + c_5E_5ch\eta_3z + c_6E_5sh\eta_3z + c_7E_7ch\eta_3z + c_8E_7sh\eta_3z + c_9 \frac{-G_sA_sI_8}{GI_{G4}I} + c_{10} \frac{G_sA_sI_8}{GI_{G4}I} + \frac{-I_8}{GI_{G4}I} q_y z \quad (20)$$

Substituting the solutions above into Equations (9) and (10), it's possible to derive the expressions of $\theta(z)$ and $w(z)$.

$$\theta(z) = c_1 F_1 \operatorname{ch} \eta_1 z + c_2 F_1 \operatorname{sh} \eta_1 z + c_3 F_3 \operatorname{ch} \eta_2 z + c_4 F_3 \operatorname{sh} \eta_2 z + c_5 F_5 \operatorname{ch} \eta_3 z + c_6 F_5 \operatorname{sh} \eta_3 z + c_7 F_7 \operatorname{ch} \eta_3 z + c_8 F_7 \operatorname{sh} \eta_3 z + c_9 \left(1 + \frac{-G_s A_s}{2EI} z^2 \right) + c_{10} \frac{G_s A_s}{2EI} z^2 + c_{11} z + \frac{-q_y}{6EI} z^3 \quad (21)$$

$$w(z) = c_1 \frac{F_1}{\eta_1} \operatorname{sh} \eta_1 z + c_2 \frac{F_1}{\eta_1} \operatorname{ch} \eta_1 z + c_3 \frac{F_3}{\eta_2} \operatorname{sh} \eta_2 z + c_4 \frac{F_3}{\eta_2} \operatorname{ch} \eta_2 z + c_5 \frac{F_5}{\eta_3} \operatorname{sh} \eta_3 z + c_6 \frac{F_5}{\eta_3} \operatorname{ch} \eta_3 z + c_7 \frac{F_7}{\eta_4} \operatorname{ch} \eta_3 z + c_8 \frac{F_7}{\eta_4} \operatorname{sh} \eta_3 z + c_9 \frac{-G_s A_s}{6EI} z^3 + c_{10} \left(z + \frac{G_s A_s}{6EI} z^3 \right) + c_{11} \frac{1}{2} z^2 + c_{12} + \frac{-q_y}{2G_s A_s} z^2 + \frac{-q_y}{24EI} z^4 \quad (22)$$

Among Equations (18)–(22), $B_1 \sim B_7$, $D_1 \sim D_7$, $E_1 \sim E_7$ and $F_1 \sim F_7$ are the coefficients related to $\eta_1 \sim \eta_4$, $I_1 \sim I_4$ and $I_{G1} \sim I_{G4}$. The arbitrary coefficients c_1, \dots, c_{12} are determined using the independent boundary conditions.

1.5. Common natural boundary conditions

According to Equations (11)–(15), the specific boundary conditions of the CW-SBS box girder can be set. For the simply supported CW-SBS box girder, the boundary conditions are as follows:

1. Uniform load.

$$w(z)|_0^l = 0; \theta'(z)|_0^l = 0; u_1'(z)|_0^l = 0; u_2'(z)|_0^l = 0; u_3'(z)|_0^l = 0; u_4'(z)|_0^l = 0 \quad (23)$$

2. Concentrated load.

As shown in Figure 3, the adjacent boundary distances to concentrated force P_k are L_1 and L_2 ; the subscripts of $w(z)$ and $\theta(z)$

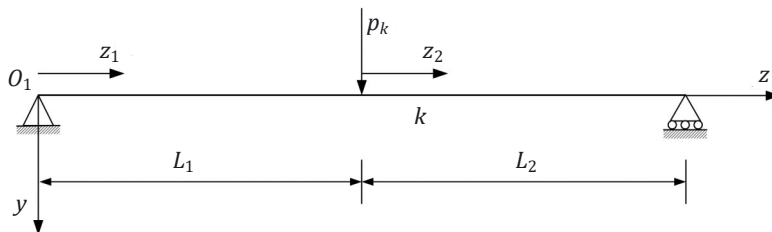


Figure 3. The coordinate and load system of a CW-SBS box girder

represent the coordinate system z_1 or z_2 . Then, the boundary condition at point k is

$$\begin{aligned} w_1(L_1) &= w_2(0); w_1'(L_1) = w_2'(0); u_{11}(L_1) = u_{12}(0); u_{11}'(L_1) = u_{12}'(0); \\ u_{21}(L_1) &= u_{22}(0); u_{21}'(L_1) = u_{22}'(0); u_{31}(L_1) = u_{32}(0); u_{31}'(L_1) = u_{32}'(0); \\ u_{41}(L_1) &= u_{42}(0); u_{41}'(L_1) = u_{42}'(0); \theta_1'(L_1) = \theta_2'(0); \theta_1(L_1) - \theta_2(0) = \frac{P_k}{G_s A_s} \end{aligned} \quad (24)$$

2. Experimental and simulative verification of the MFMSL method

Referring to the actual bridge, the experimental CW-SBS box girder model is made following the similarity principle, as shown in Figure 4a. The corrugated steel webs (Figure 4b) and steel bottom plates are made of high-quality Q345 steel whose Young's modulus is $E_s = 206$ MPa and Poisson's ratio is $\nu_s = 0.26$, their thickness is 0.3 cm and 0.4 cm, respectively. The roof and diaphragm are made of C50 concrete whose Young's modulus is $E_c = 34.5$ MPa and Poisson's ratio is $\nu_c = 0.17$, the

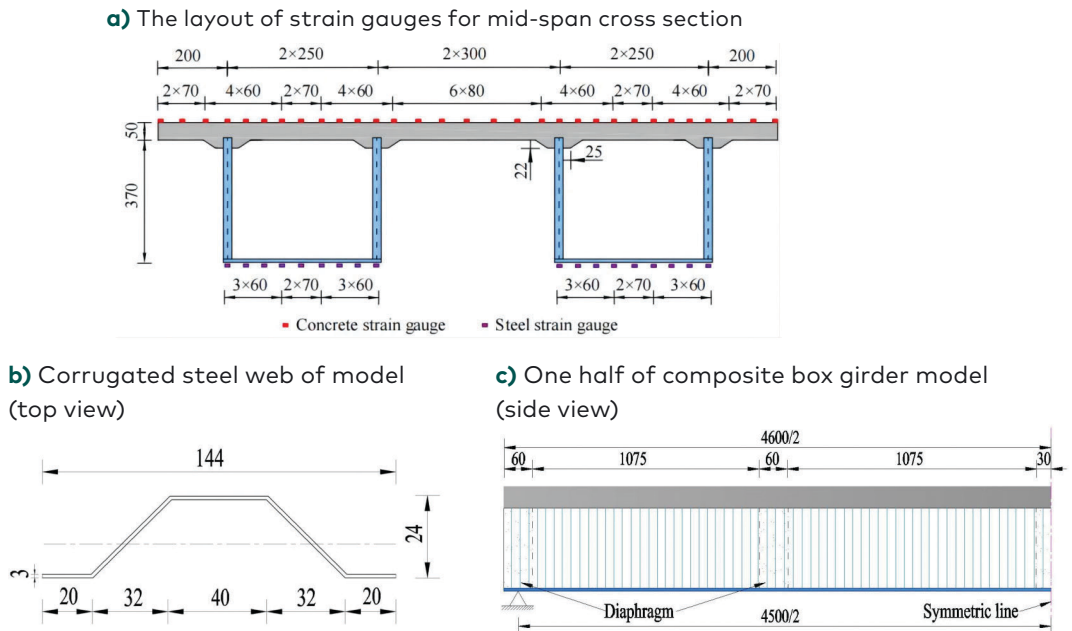


Figure 4. The dimensions and configurations of the CW-SBS model (units in mm)

average thickness is 5.5 cm, and $b_1 = 0.2$ m, $b_2 = 0.25$ m, $b_3 = 0.3$ m. The corrugated steel webs connect the upper flange using the embedded connecting keys, while the lower flange (steel bottom plate) is welded with corrugated steel webs. The dimensions and configurations of the CW-SBS box girder are shown in Figure 4. In this analysis, the density of uniformly distributed load is $q_k(z) = (11 \times 9800)/4.5$ N/m, and the concentrated load is $P_k(z) = 10 \times 9800$ N, respectively, as shown in Figure 5.

The spatial finite element model of composite box girder is established by using ANSYS software. The top and bottom slabs use SOLID65 elements; the diaphragm uses SOLID45 elements; the corrugated steel webs use SHELL63 elements; the top and bottom slabs are connected with corrugated steel webs by a common joint mode. The finite element model of the experimental CW-SBS box girder model is shown in Figure 6.

Here, the accordion effect is presented by the stress difference between corrugated steel webs and flat steel webs with equal thickness, and its ratio to the calculated stress of composite box girder with flat steel webs. The shear lag coefficient is the ratio of the theoretical value in this paper to the theoretical value of the elementary beam. Figures 7–9 show the stress distributions of steel bottom plate and



Figure 5. Testing load application and mechanical property test

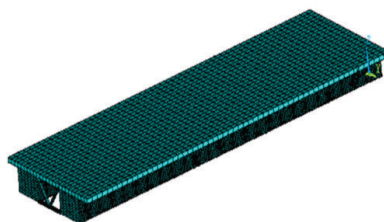


Figure 6. The finite element analysis model of the experimental CW-SBS model

the change of accordion effect under two types of loads. In the vertical bending state of the model, it can be seen that:

1. The shear lag effect is related to the load distribution. For the steel bottom plate, the shear lag coefficients at the intersection of the steel bottom plate and the web and the steel bottom plate centre are 1.25 and 0.28, respectively, the maximum value of the calculated value of tensile stress is 81.4 MPa and the minimum value is 18.2 MPa under concentrated load (Figure 7). The shear lag coefficients are 1.01 and 0.97 under uniformly distributed load (Figure 8). This shows that the stress distribution of steel bottom plate under the influence of shear lag effect is uneven, and the stress concentration is more serious under concentrated load, while the stress concentration is relatively small under uniform load.

2. The accordion effect is also related to the load distribution form. The accordion effect of steel bottom plate under the uniform load is 15.3%, and the accordion effect is uniformly distributed. While the accordion effect under the concentrated load is obviously increased and presents a curve change, the minimum value of accordion effect is 19.4% and the maximum value is 26.3% (Figure 9). Compared with the composite box girder with flat steel webs, the tensile stress of steel bottom plate significantly increases due to the influence of accordion effect. For example, at the intersection of the steel bottom plate and the web, the accordion effect increases the tensile stress by 26.3% under concentrated load. Therefore, the designer should pay attention to this phenomenon.

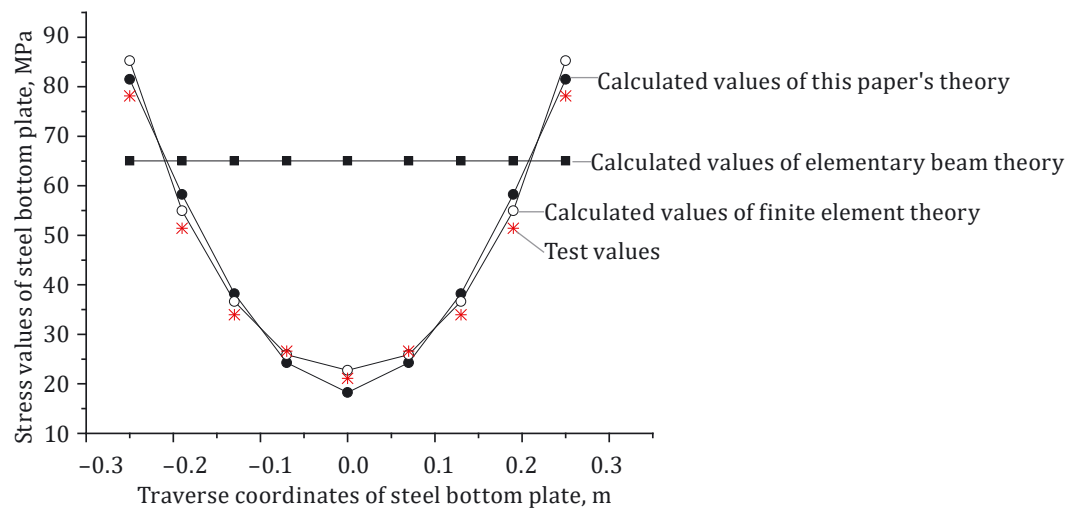


Figure 7. The stresses of steel bottom plate under the concentrated load

3. Similarly, the finite element method (FEM) accordion effect is presented by the FEM stress difference between corrugated steel webs and flat steel webs with equal thickness, and its ratio to the FEM stress of composite box girder with flat steel webs (Figure 9). Compared with theoretical values under concentrated load, the error of accordion effect is 7.5% at the centre of the cross section of the steel bottom plate, and compared with theoretical values under uniformly distributed load, the error is 7.8%. Moreover, in Figure 8, the stress error between this theory and the finite element under uniform load is within the range of 4.5%. Therefore, the theoretical values in this paper are basically consistent

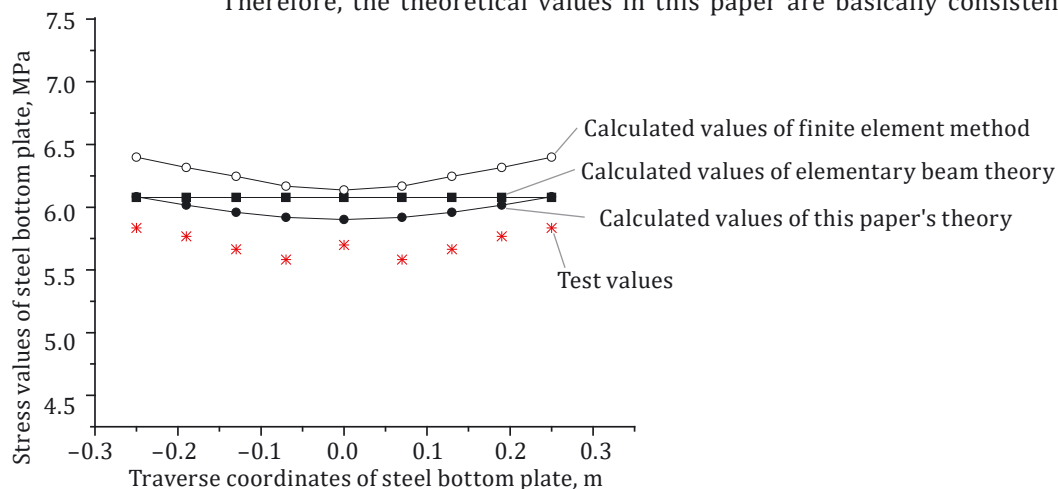


Figure 8. The stresses of steel bottom plate under uniform load

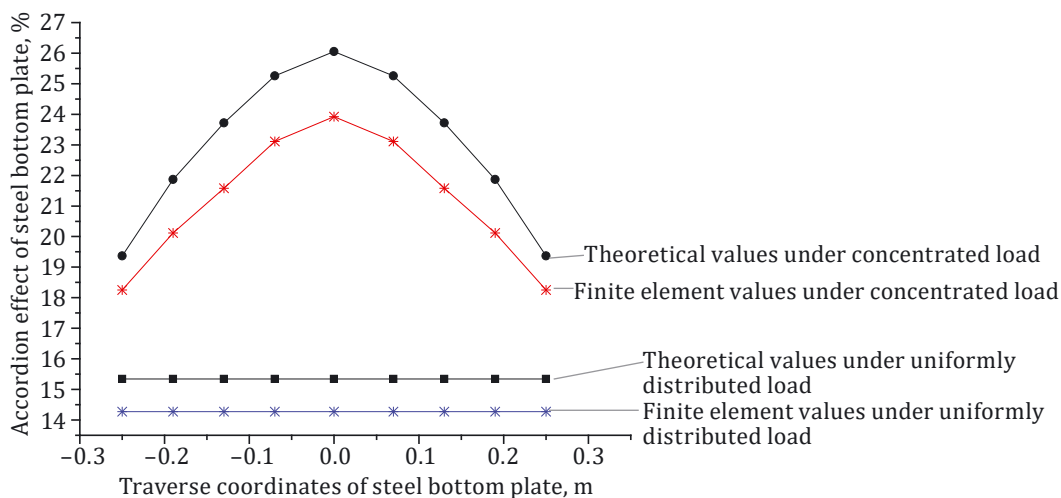


Figure 9. The accordion effect of steel bottom plate

with the finite element method, which further proves the effectiveness of this theory.

Figures 10–11 show the stress distributions of upper flange and the accordion effect change. It can be seen that:

1. Compared with the steel bottom plate, the accordion effect of upper flange is reduced, such as 10.5% under the uniform load. Similarly, the accordion effect of upper flange is closely related to the load distribution, such as 12.32% at the intersection of upper flange and web, while 22.78% at the transverse centre of upper flange under the concentrated load (Figure 11). Then, compared with the composite box girder with flat steel webs, the compressive stress of the CW-SBS box girder at the intersection of the upper flange and the web is reduced by 12.32%, and 22.78% at the transverse centre of upper flange due to the influence of accordion effect, which should also attract the attention of bridge experts.

2. The shear lag effect of upper flange is also reduced. For example, the shear lag coefficient at the intersection of upper flange and web is 1.11 under the concentrated load, while the transverse centre of upper flange is 0.383. The maximum value of the calculated value of compressive stress is 2.75 MPa and the minimum value is 0.98 MPa under concentrated load (Figure 10). However, based on the traditional shear lag theory, the shear lag coefficient of the upper flange should be the same as that of the steel bottom plate. The self-equilibrium condition of shear lag warping stress is considered in this paper, and the four longitudinal displacement difference functions are used to model the variation of shear lag in the CW-SBS box girders with different wing slab

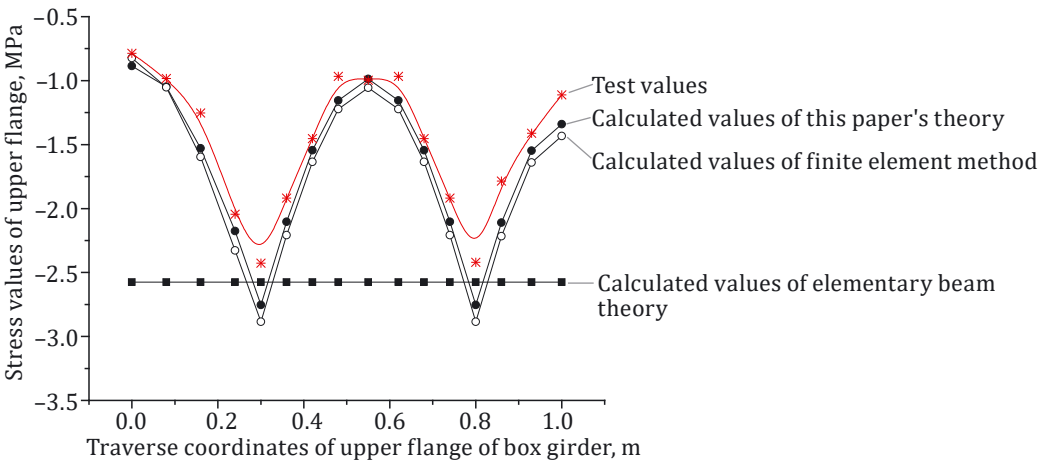


Figure 10. Stress of upper flange under concentrated load

widths and thicknesses. Therefore, the calculation accuracy of this paper is significantly improved.

3. Because the main mass of CW-SBS box girders is concentrated in the upper part, which makes the neutral axis moved up. Here, the stress at the transverse centre point of steel bottom plate is 18.6 times as much as that at the corresponding position of upper flange, and the stress at the intersection of steel bottom plate and web is 29.6 times as much as that of upper flange (Figures 7 and 10). The design strength ratio of steel bottom plate and upper flange material is 12.1 in China, which may lead to yield failure of steel bottom plates, first. Therefore, this phenomenon

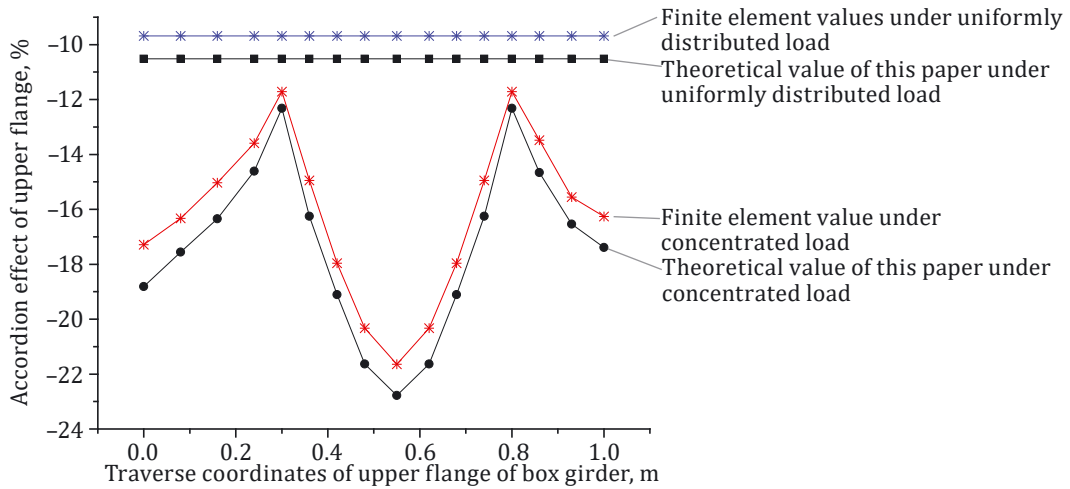


Figure 11. Accordion effect of upper flange

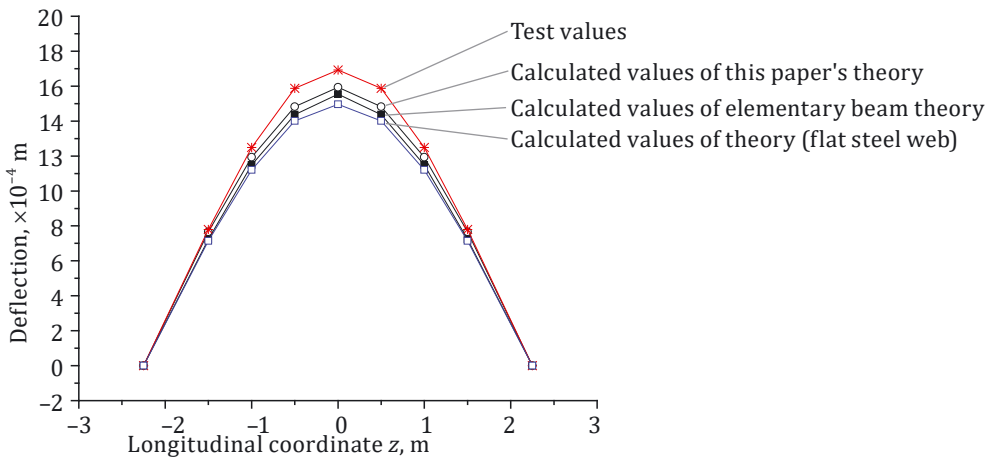


Figure 12. Deflections for simply supported composite box girder (concentrated load, $L_1=L_2=2.25$ m)

should be considered by the bridge designer, and it is necessary to rely on prestressed tendons to improve the stress condition of upper flange and steel bottom plate.

Figure 12 shows the vertical deflection of the experimental CW-SBS box girder model. It can be seen that the deflection increases slightly under the influence of shear lag and accordion effect, its influence is not prominent. For example, the influence of accordion effect on deflection is about 5.7%, while the influence of shear lag effect is 3.5% under concentrated load. In other words, the shear lag and accordion effect have minute effect on the overall stiffness of the CW-SBS box girder model.

Conclusions

1. As shear lag, shear lag warping stress self-equilibrium condition and accordion effect have been considered comprehensively, the theoretical basis of this paper is more solid. Moreover, the calculated results of the MFMSL method are in good agreement with the numerical simulation and test results, which show that the MFMSL method is effective. Hence, the MFMSL method presented in this paper is of high theoretical and practical significance. In particular, the proposed MFMSL method contributes to the theoretical foundation for the design of CW-SBS box girder bridge.
2. The study shows that the shear lag effect of CW-SBS box girder is obvious, and the shear lag effect is related to the load distribution. Under concentrated load, the shear lag effect of CW-SBS box girder is more prominent, and the shear lag coefficient at the intersection of the steel bottom plate and the web is the largest, while the shear lag coefficient at the centre of steel bottom plate is the smallest. In particular, compared with the upper flange, the shear lag effect of steel bottom plate is more significant. This shows that the stress distribution of steel bottom plate and upper flange under the influence of shear lag effect is uneven, and the stress concentration is more serious under concentrated load, while the stress concentration is relatively small under uniform load.
3. This paper has investigated the accordion effect of CW-SBS box girder, and the accordion effect of traditional composite box girder is generally not more than 10%, such as the Cognac Bridge in France. However, the accordion effect of the CW-SBS box girder is significantly increased, and the accordion effect is also related to the load distribution form. Under concentrated load, the accordion effect of CW-SBS box girder is more obvious. It is particularly noteworthy that the accordion effect of CW-SBS box girder reduces

the compressive stress of the upper flange and increases the tensile stress of the steel bottom plate.

4. The MFMSL method effectively improves the calculating accuracy of the CW-SBS box girder static response, and the CW-SBS box girder has the advantages of mechanics and materials. Compared with PC box girder bridge, the weight of the CW-SBS box girder is further reduced by about 50% and the steel bottom plate is free from concrete pouring. Also, the temperature stress, shrinkage and creep are effectively controlled. In particular, this kind of bridge is more suitable for the construction of bridges in high-intensity seismic areas, as well as soft soil and collapsible loess areas. Hence, this study further presents the good prospects of CW-SBS box girder bridges in the world.

FUNDING

The research has been financially supported by the National Natural Science Foundation of China under Grant 514789408; the Science and Technology Plan of Gansu Province of China under Grant 19ZD2GA002.

REFERENCES

- Aparna, P., & Varghese, B. (2020). Seismic analysis of composite box girders with corrugated steel webs and trusses. In R.M. Singh, K.P. Sudheer, & B. Kurian (Eds.), *Advances in Civil Engineering*, 83, (pp. 261–277). Springer, Singapore. https://doi.org/10.1007/978-981-15-5644-9_18
- Chen, Y., Dong, J., Xu, T., Xiao, Y., Jiang, R., & Nie, X. (2019). The shear-lag effect of composite box girder bridges with corrugated steel webs and trusses. *Engineering Structures*, 181, 617–628. <https://doi.org/10.1016/j.engstruct.2018.12.048>
- Deng, W., Liu, D., Peng, Z., & Zhang, J. (2021). Behavior of cantilever composite girder bridges with CSWs under eccentric loading. *KSCE Journal of Civil Engineering*, 25(10), 3925–3939. <https://doi.org/10.1007/s12205-021-2328-3>
- Elgaaly, M., Seshadri, A., & Hamilton, R. W. (1997). Bending strength of steel beams with corrugated webs. *Journal of Structural Engineering*, 123(6), 772–782. [https://doi.org/10.1061/\(ASCE\)0733-9445\(1997\)123:6\(772\)](https://doi.org/10.1061/(ASCE)0733-9445(1997)123:6(772))
- Gomez, H. C., Fanning, P. J., Feng, M. Q., & Lee, S. (2011). Testing and long-term monitoring of a curved concrete box girder bridge. *Engineering Structures*, 33(10), 2861–2869. <https://doi.org/10.1016/j.engstruct.2011.05.026>
- He, J., Liu, Y., Chen, A., & Yoda, T. (2012). Mechanical behavior and analysis of composite bridges with corrugated steel webs: state-of-the-art. *International Journal of Steel Structures*, 12(3), 321–338. <https://doi.org/10.1007/s13296-012-3003-9>

- He, Z.-Q., Li, Y., Xu, T., Liu, Z., & Ma, Z. J. (2021). Crack-based serviceability assessment of post-tensioned segmental concrete box-girder bridges. *Structures*, 30,1097–1108. <https://doi.org/10.1016/j.istruc.2021.01.062>
- Jiang, R. J., Au, F. T. K., & Xiao, Y. F. (2014). Prestressed concrete girder bridges with corrugated steel webs: review. *J. Struct. Eng.*, 141(2), Article 04014108. [https://doi.org/10.1061/\(ASCE\)ST.1943-541X.0001040](https://doi.org/10.1061/(ASCE)ST.1943-541X.0001040)
- Kim, H.-J., Kim, H.-K., & Park, J. Y. (2013). Reliability-based evaluation of load carrying capacity for a composite box girder bridge. *KSCE Journal of Civil Engineering*, 17(3), 575–583. <https://doi.org/10.1007/s12205-013-0603-7>
- Limongelli, M. P., Chatzi, E., & Anzlin, A. (2018). Condition assessment of roadway bridges: From performance parameters to performance goals. *The Baltic Journal of Road and Bridge Engineering*, 13(4), 345–356. <https://doi.org/10.7250/bjrbe.2018-13.421>
- Mo, Y. L., Jeng, C.-H., & Chang, Y. S. (2000). Torsional behavior of prestressed concrete boxgirder bridges with corrugated steel webs. *ACI Struct. J.*, 97(6), 849–859. <https://doi.org/10.14359/9630>
- Oh, J.-Y., Lee, D. Y., & Kim, K. S. (2012). Accordion effect of prestressed steel beams with corrugated webs. *Thin-Walled Structures*, 57, 49–61. <http://dx.doi.org/10.1016/j.tws.2012.04.005>
- Shen, K., Wan, S., Mo, Y. L., Song, A., & Li, X. (2018). Behavior of single-box multi-cell box-girders with corrugated steel webs under pure torsion. Part I: Experimental and numerical studies. *Thin-Walled Structures*, 129, 542–557. <https://doi.org/10.1016/j.tws.2017.10.038>
- Yong, D., Jiang, K., & Liu, Y. (2012). Nonlinear analysis for PC box-girder with corrugated steel webs under pure torsion. *Thin-Walled Structures*, 51(2), 167–173. <https://doi.org/10.1016/j.tws.2011.10.013>
- Zeying, A., Liu, J., Qu, J., Zhou, X., & Li, L. (2015). Temperature field of PC box girder bridge based on GPRS temperature collection system. *Wuhan University Journal of Natural Sciences*, 20(3), 269–276. <https://doi.org/10.1007/s11859-015-1092-y>
- Zhang, G., Kodur, V., Xie, J., He, S., Hou, W. (2017). Behavior of prestressed concrete box bridge girders under hydrocarbon fire condition. *Procedia Engineering*, 210, 449–455. <https://doi.org/10.1016/j.proeng.2017.11.100>
- Zhao, C., Zhou, Y., Zhong, X., Wang, G., Yang, Q., & Hu, X. (2022). A beam-type element for analyzing the eccentric load effect of box bridges. *Structures*, 36, 1–12. <https://doi.org/10.1016/j.istruc.2021.11.001>
- Zhou, C., Li, L., Wang, L. (2019). Improved softened membrane model for prestressed composite box girders with corrugated steel webs under pure torsion. *Journal of Constructional Steel Research*, 153, 372–384. <https://doi.org/10.1016/j.jcsr.2018.10.023>
- Zhou, M., Liu, Z., Zhang, J., An, L., & He, Z. (2016). Equivalent computational models and deflection calculation methods of box girders with corrugated steel webs. *Engineering Structures*, 127, 615–634. <http://dx.doi.org/10.1016/j.engstruct.2016.08.047>